ELSEVIER

Earth and Planetary Science Letters 176 (2000) 311–321

EPSL

www.elsevier.com/locate/epsl

The core–mantle boundary under the Gulf of Alaska: No ULVZ for shear waves

John C. Castle *, Rob D. van der Hilst

Massachusetts Institute of Technology, Cambridge, MA, USA

Received 23 November 1999; accepted 25 January 2000

Abstract

The Earth's core–mantle boundary (CMB) marks the boundary between the hot, molten iron core and the silicate mantle and is a thermal, chemical, and flow boundary. Previous observations of very slow compressional wavespeeds suggest that thin ultra-low-velocity zones (ULVZs), possibly composed of a mixture of molten iron and silicates, exist at the base of the mantle. A molten or partially molten layer would cause a large shear wavespeed decrease; however this velocity drop has not been observed. Here, we use core reflected *ScP* phases to investigate the shear properties of ULVZs. These phases reveal at least two distinct regions: one region under Central America which is distinctly average (PREM and iasp91-like) and a second region under the entire Gulf of Alaska that produces large *ScP* reflections with amplitudes of up to 30 times larger than calculated with average Earth models. The large amplitudes suggest a combination of focusing by CMB topography, high shear wavespeeds at the bottom of the mantle, and low attenuation (high Q) along the *ScP* path; high shear wavespeeds and low attenuation are opposite from what would be expected from a shear wave ULVZ. A ULVZ in compressional wavespeeds (ultra-low V_p) has previously been observed in this region; however, in addition to the large amplitudes, the short-period *ScP* waveforms show no complexity that can be related to a ULVZ. Thus, either there is not a ULVZ under the Gulf of Alaska or, if it does exist, it is restricted to compressional wavespeed changes, precluding interpretation as partial melt but rather suggesting a chemical origin.

Keywords: core-mantle boundary; low-velocity zones; mantle; seismology; convection; partial melting

1. Introduction

The core-mantle boundary (CMB), where the solid mantle silicates meet the molten iron core, is a thermal boundary where wavespeeds and electrical properties are discontinuous [1]. At this boundary anomalous seismic observations suggest the existence of thin, regional ultra-low-velocity zones (ULVZs) (e.g. [2,3]) which may contain partial melt [4,5]. The implications of a partially molten zone are large: for example, it may be related to the origin of hotspots and may influence the direction of magnetic reversal paths (see [2,3] for comprehensive reviews).

Enigmatically, there is no evidence for the existence of the large drop in shear wavespeeds that would accompany a ULVZ with partial melt. This may be due partially to the limitations of earth-

* Corresponding author. E-mail: castle@mit.edu

0012-821X/00/$ – see front matter
PII: S0012-821X(00)00027-3

quake/receiver distribution. Two regions that can be investigated for shear and compressional wave ULVZs (we introduce the terms ULV_sZ and ULV_pZ for a V_s ULVZ and a V_p ULVZ, respectively) are beneath the Gulf of Alaska in the northwest Pacific and beneath northern Central American. In these regions, compressional wave studies find that the CMB beneath northern Central America appears devoid of ULV_pZs [2] while a ULV_pZ exists beneath the Gulf of Alaska [6].

The core reflected *ScP* phase (Fig. 1) can be used to search for ULV_sZ structure because the changes in shear wavespeed expected at a partial melt ULVZ would create observable pre- and post-cursors to *ScP* [7]. Previously, *ScP* waveforms from two earthquakes show that one point at the CMB beneath the Gulf of Alaska near 205°E and 55°N is 'sharp' and without structure [8]. However, extending this work globally is difficult as *ScP* is most often a small amplitude phase buried in the noise, thus limiting *ScP* waveform studies.

In this study, we expand on the Vidale and Benz (1992) [8] study by collecting and stacking data from many earthquakes recorded at a dense seismic network. Similar to their study, we model *ScP* and *P* waveform complexities. Extending beyond their work, the inclusion of more earthquakes allows us to investigate larger regions. Additionally, we observe and attempt to explain large variations of *ScP* amplitude. Finally, we interpret our results in the context of possible ULVZ structures. We find that the *ScP* amplitudes from Central American earthquakes are comparable to predicted amplitudes while *ScP* amplitudes from Alaskan earthquakes are much larger than expected compared to synthetics, opposite from what is expected from a ULVZ. Furthermore, the large *ScP* amplitudes facilitate waveform analysis which we exploit to investigate whether the kind of waveform complexities that would be produced by an ULV_sZ can be detected in the data.

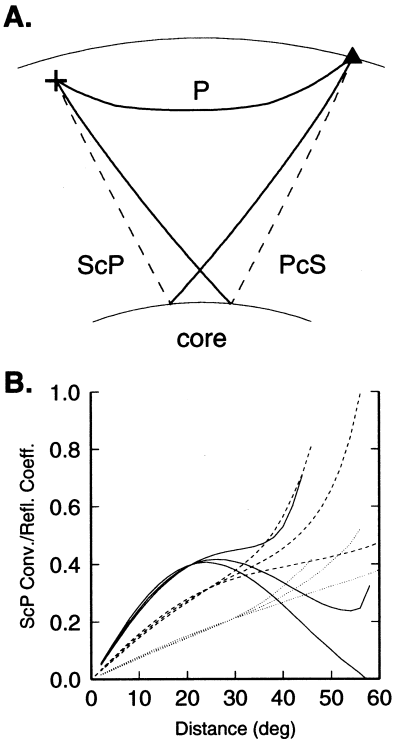

Fig. 1. (A) The *P*, *PcS*, and *ScP* waves from an earthquake at 200 km depth and a station at 30° distance. (B) The *S*-to-*P* conversion and reflection coefficient versus distance. The middle dashed line shows the iasp91 model. The upper/lower dashed line is for $\Delta V_p = +/-10\%$ at the CMB with an iasp91 V_s contrast. The solid/dotted lines are for $\Delta V_s = +/-30\%$, with the upper/lower line in each group a 10% V_p increase/decrease.

2. Seismic data and absolute *ScP* amplitudes

The Pacific northwest seismic network (PNSN) in Washington and Oregon is a large aperture, triggered, short-period, vertical component seismic network that routinely records local seismic activity in the western United States. PNSN also records teleseismic events when amplitudes are large enough to 'trigger' the network. The triggering mechanism activates when several seismic stations measure large amplitudes at similar times and the length of the time window saved is proportional to the amplitude of the triggering signal. These data are made publicly available at the Incorporated Research Institutions for Seismology Data Management Center (IRIS DMC). The *ScP* phase arrives roughly 7 min after the *P* wave and usually has an amplitude $< 10\%$ of

Table 1
22 earthquakes

No.	Date	Location		Depth (km)	M_b	Sta. (#)	Δ (°)	Bot. dep.	Nodal?	noise/*P* amp.	*PcP* seen?	*ScP* seen?	*ScP*/*P* amp.		
		°N	°E										data	syn.	ratio
Aleutian earthquakes to PNSN															
1	1987-03-21	52.0	182.5	100	5.9	77	36	890		0.15	–	good	0.72	0.12	6
2	1987-08-14	53.4	190.9	114	5.7	63	31	794		0.18	–	good	0.35	0.07	5
3	1988-02-07	60.3	206.7	136	6.2	116	23	696	*P*	–	–	–	–	0.17	–
4	1988-11-30	61.4	207.5	135	6.0	82	23	695	*ScP*	0.17	–	good	0.56	0.04	13
5	1989-05-19	54.3	194.4	108	6.1	89	28	758		0.60	–	good	2.56	0.11	23
6	1990-05-01	58.8	203.2	217	6.1	77	24	707		0.11	good	good	0.53	0.04	13
7	1991-01-23	52.0	178.8	111	5.7	103	38	931		0.07	poor	good	0.32	0.08	4
8	1991-05-01	62.6	208.5	114	6.1	117	23	694	*P*	0.34	–	good	0.58	0.10	6
9	1991-08-14	54.3	190.7	287	5.7	89	31	807		0.04	–	good	0.23	0.05	5
10	1993-11-20	60.2	206.9	122	5.7	124	23	692		–	none	–	–	0.03	–
11	1994-07-14	55.4	196.2	168	5.6	79	28	758		0.08	good	fair	0.20	0.18	1
12	1995-02-12	59.6	206.6	111	5.7	49	24	701		0.17	none	good	0.36	0.03	11
Aleutian earthquakes to California BB															
13	1990-05-01	58.8	203.2	217	6.1	9	31	807	both	0.08	good	good	1.50	0.37	4
14	1993-11-20	60.2	206.9	122	5.7	10	35	862		0.25	none	good	1.55	0.06	28
Central American earthquakes to PNSN															
15	1989-09-16	16.5	266.3	113	6.0	109	38	923		–	–	–	–	0.11	–
16	1991-03-01	10.9	275.4	205	6.1	117	47	1185		–	good	–	–	0.02	–
17	1994-03-14	15.9	267.6	163	5.8	127	39	963		0.08	poor	none	0.16	0.30	1
18	1995-10-21	16.8	266.5	161	6.0	133	38	931		0.07	none	none	0.23	0.06	4
19	1996-12-31	15.9	267.1	107	6.0	130	39	947		–	poor	–	–	0.08	–
20	1997-11-09	13.9	271.2	194	6.0	130	43	1054		–	fair	–	–	0.10	–
21	1997-12-18	13.9	271.3	170	6.0	130	43	1050		–	fair	–	–	0.08	–
Central American earthquakes to California BB															
22	1997-11-09	13.9	271.2	176	6.0	21	38	916		0.04	poor	none	0.30	0.11	3

California BB includes the broadband stations from the northern California seismic network and terrascope network ellipse indicate that the PNSN did not save the time window.

Observation classifications are as follows: good, *ScP* is obvious; fair, *ScP* is present are can be used for alignment; poor, *ScP* seen but cannot be used for alignment; none, no *ScP* seen.

Abbreviations are as follows: Sta. (#), number of stations; Δ (°), distance in degrees; amp., amplitude; syn., synthetic; Bot. dep., bottoming depth (km) of the wave.

the *P* amplitude that does not trigger the network; therefore *ScP* is usually recorded only if the recorded *P* window is long enough.

We searched for *ScP* arrivals from earthquakes at depths greater than 100 km, with magnitudes larger than m_b 5.6, and at distances less than 50 from PNSN. From shallower earthquakes *ScP* must travel through the highly shear wave attenuating region directly below the crust. At greater distances the incident *S* angle at the CMB is overcritical for *S*-to-*P* conversion/reflections (Fig. 1). For *ScP* to be recorded at PNSN, these requirements limit earthquakes to regions beneath Central America and Alaska. Note that *PcS* arrives after *ScP* from deep earthquakes; additionally, the vertical component instruments further reduce any possibility of interference from *PcS*.

Unfortunately, most PNSN recordings of Central American earthquakes do not include the *ScP* time window (Table 1). Only for earthquakes 17 and 18 was the *ScP* time window saved (Fig. 2). The radiation patterns for these events suggest that *ScP* is not nodal (Table 1, *ScP*/*P* amplitude, synthetic), however, while the *P* wave signal-to-noise ratio for both events is clearly large, *ScP* is not visible in either recording. We also analyzed broadband records of a Central American earthquake recorded at the terrascope and northern California seismic networks. While these networks are much sparser than the short-period networks, they do record continuously. Nevertheless, these broadband records show no signs of *ScP*.

These observations contrast sharply to PNSN recordings of earthquakes occurring beneath Alaska and the Aleutian Islands. For all but two (events 3 and 10) of the earthquakes for which the *P* wave was recorded, the *ScP* phase was also large enough to trigger the network, even if the intermediate *PcP* time window was not saved. The *ScP* amplitudes from these earthquakes are comparable to *P* amplitudes. Fig. 2 shows six unfiltered seismograms from three Alaskan earthquakes recorded at PNSN. In these raw data, the *ScP* phase arrives within one second of the iasp91 predicted arrival time but the amplitude of *ScP* is an order of magnitude larger than expected from synthetic seismograms incorporating focal mechanisms. We also investigated

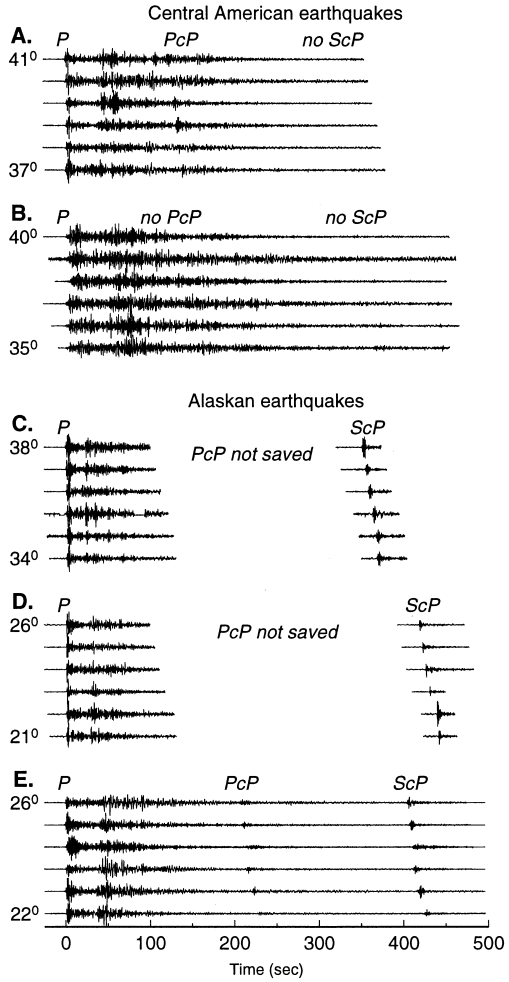

Fig. 2. A subset of unfiltered short-period vertical component seismograms from events 17 (A) and 18 (B), where no *ScP* is seen, and events 1 (C), 4 (D), and 6 (E), where *ScP* is seen. All traces are normalized to the *P* amplitude.

two Alaskan earthquakes recorded at the California broadband networks. These broadband data show similarly large *ScP* amplitudes.

Fig. 3 maps the region we have investigated. Yellow diamonds and red circles mark the *ScP* reflection points: red circles indicate that *ScP* was saved while yellow diamonds indicate that *ScP* was not saved by PNSN. No systematic dependence of *ScP* amplitude on earthquake magnitude or distance can be identified in the data. However, we note the markedly large amplitudes

of *ScP* from Alaskan earthquakes: these absolute amplitudes are consistently large enough to trigger the PNSN network.

3. Data analysis and *ScP* modeling

In order to model the amplitudes of the *ScP* phase relative to the *P* wave, we created complete 2 s period direct solution method (DSM) synthetic seismograms [9] using the iasp91 velocity model [10], the PREM attenuation model [11], and the USGS radiation patterns [12]. We employ the iasp91 velocity model to calculate travel times as it is most frequently used for 1 Hz body waves; however, using the PREM velocity model would change the *ScP–P* differential travel time by a negligible 0.01 s. Table 1 (*ScP/P* synthetic amplitude) lists the relative *ScP/P* amplitudes in the synthetic data, computed by taking the median ratio of the *ScP* peak absolute amplitude to the *P* peak absolute amplitude in each synthetic seismogram. The Central American and Alaskan synthetic amplitudes are equally large, suggesting that radiation patterns cannot explain the differences in observed amplitudes. Note that the double-couple radiation patterns suggest that nodal lines, directions at which no energy is emitted from the earthquake, pass through PNSN for four events (Table 1). While the use of the complete moment tensor and non-ray synthetics partially mitigate this complexity, relative amplitudes for events 3, 4, 8, and 13 should therefore be viewed somewhat tenuously.

Insofar that we have only three measurements, that the synthetic reproduce the three measured Central American *ScP/P* amplitudes fairly well (in comparison to the Alaskan observations) suggests that the PREM attenuation model and the iasp91 velocity model provide a reasonable description of the Earth beneath Central American. However, for Alaskan earthquakes the synthetic *ScP* signals are roughly one order of magnitude smaller than the observed *ScP* amplitudes: these models poorly describe the Earth under the Gulf of Alaska. These large *ScP* amplitudes could be due to several mechanisms: topography on the CMB to focus *ScP*, an increase in the *S*-to-*P* conversion/reflection coefficient at the CMB, less attenuation of *ScP*, and more attenuation of the *P*.

Kirchoff synthetic calculations of 1 s period *PcP* amplitudes reflecting of off a CMB with sinusoidal topography similar to an 'egg-crate' yield two observations [13]: small-scale topography at horizontal length scales less than 50 km decreases *PcP* amplitudes for all take-off angles and large-scale topography alternately focuses and defocuses energy reflecting at the topographic lows and highs, respectively. In the latter case, the peak amplitude enhancement is $\sim$50% and occurs when the topography length scale equals the Fresnel zone, with radius $\sim$200 km for 2 s period *ScP* (Fig. 3). The maximum focusing of *ScP* occurs when the CMB topography coincides with the *ScP* isochron shape, which is approximately the shape of an elongated 'bowl' with vertical topography of $\sim$1.4 km over a span of 100 km horizontally.

If one large bowl-shaped depression focused energy for all of the Alaskan events, it would span over 20° horizontally and thus, to remain roughly bowl-shaped, include an unreasonable amount (over 30 km) of CMB topography. Moreover, while four Alaskan earthquakes with little or no *ScP* signal (events 3, 9, 10, and 11) suggest some small-scale topography, the overall large amplitudes argue against a dominant 'egg-crate' variation of the CMB depth but instead suggest an east/west oriented trough-like CMB depression. In any case, the analysis of *PcP* amplitudes [13] suggests that topography can only increase *PcP* or *ScP* amplitudes by up to 50% and not by the order of magnitude inferred from the data.

The *S*-to-*P* conversion/reflection coefficient depends on the velocity and density contrasts across the boundary between the solid mantle and liquid outer core. The mantle density and outer core compressional wavespeed (V_p) and density have a minor effect on the coefficient: increasing core density or velocity would slightly decrease the coefficient and increasing mantle density would slightly increase the coefficient. Increasing either V_p or V_s at the base of the mantle increases the coefficient; decreasing either V_p or V_s decreases the coefficient (Fig. 1). Most of the Alaskan earthquakes occurred near 26°. At these distances a

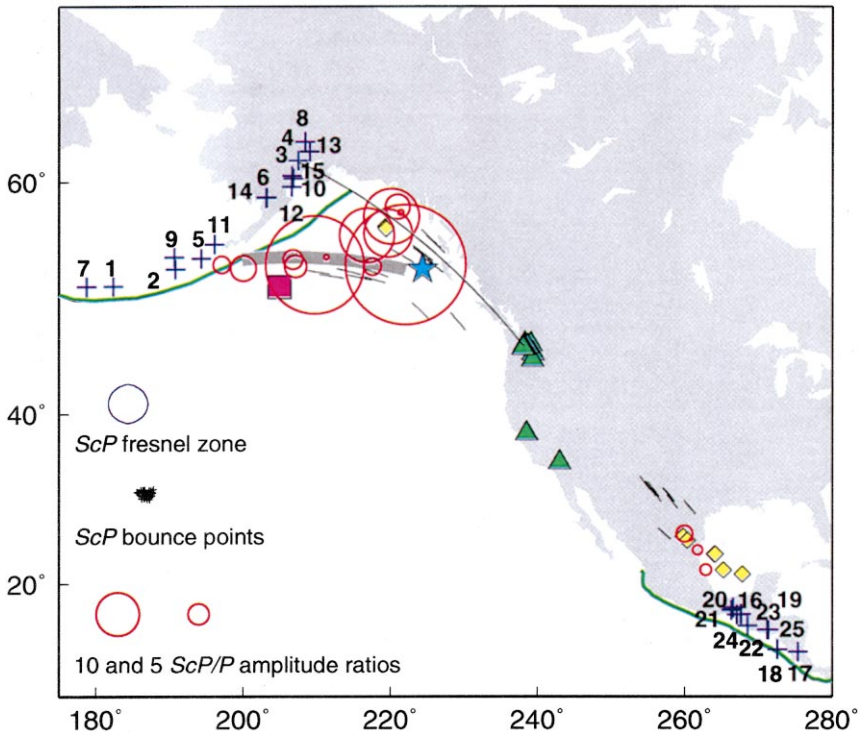

Fig. 3. Map of earthquake locations (crosses), mean station locations (triangles), and *ScP* reflection points (yellow diamonds and red circles). Yellow diamonds indicate that the *ScP* time window was not saved while red circles show recorded *ScP* phases. Circle sizes are proportional to the observed *ScP* versus *P* amplitude ratio relative to the synthetic ratio. The star marks the Bowie seamount and the magenta square marks the *ScP* reflection point of Vidale and Benz (1992) [8] (square size is not proportional to amplitude). Black lines mark the bottoming location and orientation of the *P* waves; long thin black line shows the cross-section path for Fig. 4; the thick gray line marks the P_{diff} path of SP_dKS across the CMB [6]. Lower left: the blue circle shows the Fresnel zone for the *ScP* travel time at a frequency of 0.5 Hz; black crosses schematically mark the *ScP* reflection points for one earthquake recorded at PNSN, and the red circles show the *ScP*/*P* scale.

30% increase in mantle V_s increases the coefficient by ~25%. Conversely, a 30% decrease in V_s decreases the coefficient by ~40%, regardless of the V_p change. Indeed, most tomographic models of the lower mantle suggest fast V_s and moderate to slow V_p wavespeeds beneath the Gulf of Alaska (e.g. [14,15]); however the increases in V_s wavespeed are of order 2–3%, suggesting only minor increases in the *S*-to-*P* conversion/reflection coefficient.

Varying the attenuation along the *ScP* and *P* paths can account for some of the large amplitudes. In the PREM model, the quality factor Q_s, attenuation^{-1}, starts at 600 in the crust, drops to 80 beneath the crust, and increases to 143 and 312 in the upper and lower mantles. Setting Q_s to either 312 or 600 throughout the entire mantle results in *ScP* amplitude increases of 50% and 300%, respectively. While low attenuation with $Q_s = 600$ or higher is plausible at 1 Hz frequencies in the lower mantle [16,17], Q_s values above 600 are likely too large for the upper mantle, especially considering that long-period maps of upper mantle attenuation show higher than average attenuation in the upper mantle beneath both Mexico and the Gulf of Alaska [18,19].

Higher attenuation of the *P* wave would result in smaller *P* amplitudes and thus larger *ScP*/*P* amplitudes. The *P* waves bottom beneath the Bowie seamount (Fig. 3, blue star). Slow velocities

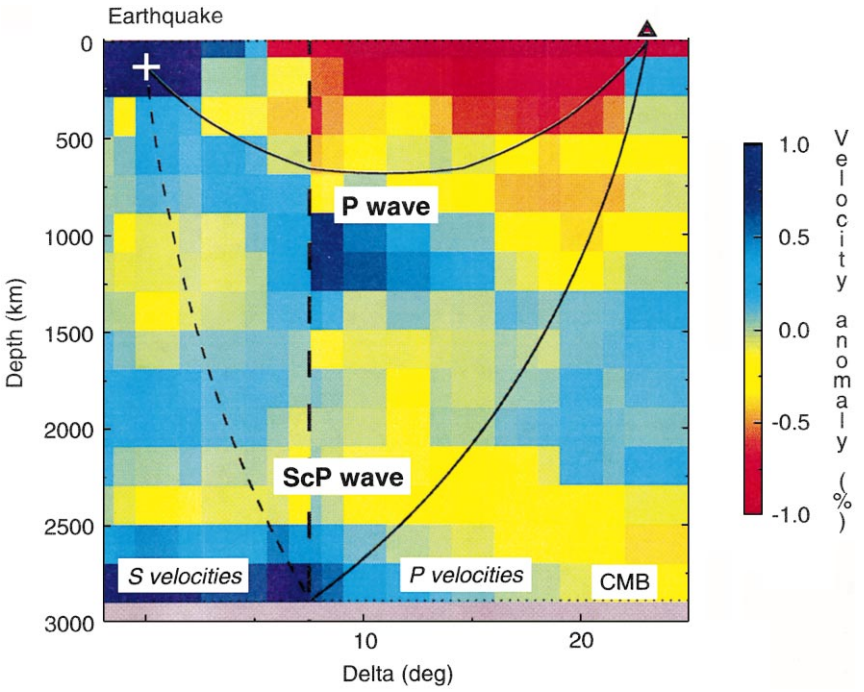

Fig. 4. The *ScP* wave and *P* wave for event 4 superimposed on the *S* wavespeed model of [21], left of 7.5°, and the *P* wavespeed model of [14]. Amplitudes greater than 1% are cropped. Travel time calculations through these models predict a 0.4 s late *P* and a 0.7 s early *ScP* for a −1.1 s residual. This compares favorably to the observed residual of −1.5 s.

below the transition zone suggest localized ponding of hot plume material near the seamount [20], which would increase *P* attenuation. Examinations of cross-sections through V_s [21] and V_p [14] mantle topography models show that most of the *ScP* phases travel through faster material while the *P* paths lie dominantly in slower material (Fig. 4). Indeed, the average differential *ScP*–*P* residual is −1.5 s, with early *ScP* arrivals and late *P* arrivals. Thus it is likely that some of the large *ScP*/*P* amplitude ratios, but not large absolute *ScP* amplitude, is due to small amplitude *P* waves.

It is unlikely that any of the factors discussed can by themselves increase the *ScP* amplitude an order of magnitude over the expected value. Instead we suggest that a combination of focusing from CMB topography, a larger *S*-to-*P* conversion/reflection coefficient due to fast V_s wavespeeds at the base of the mantle, high attenuation along the *P* path, and low attenuation along the *ScP* path can together create the anomalous *ScP* amplitudes.

4. ULV_pZ but not ULV_sZ beneath the Gulf of Alaska

Tectonically, the Kula Plate has subducted beneath Alaska, suggesting that paleoslab material in the lower mantle may be responsible for the above mentioned scenario. However, although the amplitudes and lateral extent of the wavespeed variations are not well constrained by the data used, travel time tomography has revealed slower than average compressional wavespeeds in a large region at the base of the mantle beneath Alaska (e.g. [14,22,23]). Conversely, tomography has imaged faster than average *S* wave propagation in the same region (e.g. [15,21]). Indeed, joint tomographic inversions of bulk and shear wavespeeds show very anomalous ($d \ln V_\phi / d \ln V_s$)

ratios in this region, which suggest compositional variations [23,24].

Observations of anomalous SP_dKS phases [6], *PcP* precursors [25], and *PKP* precursors [26,27] suggest a thin layer of ultra-low V_p ($\Delta V_p \approx -10\%$) directly above the CMB with thickness up to 40 km. One interpretation of this dramatic drop in V_p is that ULVZs are regions of partial melt. Partial melt further implies a 3:1 V_s to V_p drop (i.e. $\Delta V_s = -30\%$ for $\Delta V_p = -10\%$) [4,5]. Large trade-offs exist between layer thickness and velocity and density changes [28] and range from $\Delta V_s = 0\%$ (no ULVZ and no partial melt) to $\Delta V_s \approx -50\%$ under Iceland [29]. One model of a partial melt zone at the base of the mantle that fits the data is 15–20 km thick and contains a -10% ΔV_p, -30% ΔV_s, and a 20% density (ρ) increase [28].

While seemingly the most obvious, the large V_s drop has not been observed anywhere. *ScP* signals should be an excellent probe as a ULV_sZ would produce two *ScP* precursors from *S*-to-*P* conversions at the topside of the ULV_sZ ($S_{ulvz}P(up)$ and $S_{ulvz}PcP$) and one coda phase from *S*-to-*P* conversions at the underside of the ULV_sZ ($ScS_{ulvz}P$) [7]. Previous investigations have been hampered by small *ScP* amplitudes; two successful studies have found either a weak signal possibly originating at an UlV_sZ under the southwestern Pacific [7] and a large *ScP* signal indicating no partial melt at one point northwest in the Gulf of Alaska [8] (Fig. 3).

Single SP_dKS raypaths showing a ULV_pZ can be modeled with an ULV_pZ above the CMB either beneath the source or beneath the receiver. For example, an SP_dKS raypath from a Indonesian earthquake recorded in North America shows signs of a ULV_pZ. This could be due to a ULVZ beneath either the northern Java Sea or the Gulf of Alaska. However, the analysis of multiple SP_dKS raypaths with similar source side paths (within 10–100 km) showing no signs of a ULV_pZ suggests that the ULV_pZ exists under the Gulf of Alaska (thick gray line, Fig. 3) [2,6]. Thus the Alaskan *ScP* data recorded at PNSN, which reflect at points ranging across the entire Gulf of Alaska, provide good coverage to probe for the ULVZ and any partial melt ULV_sZ.

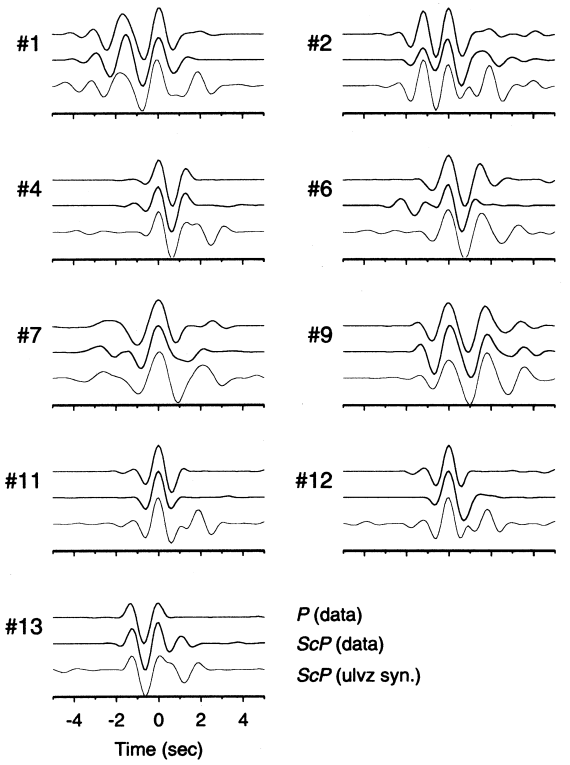

Fig. 5. Stacked data from nine earthquakes. In each group: top, the stack of the observed *P* wave; middle, the stack of the observed *ScP*; and bottom, the stacked WKBJ ULVZ *ScP* synthetics. Each individual WKBJ synthetic is convolved with the source time function (the stacked *P* wave) before stacking. In the ULVZ synthetics, $\Delta V_s = -30\%$ and the amplitude of the *ScP* post-cursor is directly proportional to ΔV_s. Synthetic *ScP* waveforms in an earth without a ULVZ would look like the *P* waveform.

To compare *P* and *ScP* waveforms we bandpass filter the data at 1–4 s periods, align on *P* (for *P* stacks) or *ScP* phase (for *ScP* stacks), and stack the data using phase-weighting stacking [30]. At lower frequencies, the arrivals are even more coherent than presented here while at higher frequencies, it becomes increasingly difficult to align the data due to varying near-receiver crustal reverberations. The *P* wave from closer events could be 'contaminated' by triplicated phases turning just below the transition zone. However, similar to previous work in this region (T. Melbourne, personal communication), we see very few signs of triplicated phases along these paths. Fig. 5 shows the stacked *P* waves and *ScP* waves

for the Alaskan earthquakes, except for events 3 and 10 (no data) and 5 and 8 (emergent P waves that we could not align). The P and ScP waveforms are strikingly similar, suggesting a simple CMB without a ULVZ.

Furthermore, Fig. 5 shows comparisons between the observed data and WKBJ synthetic seismograms [31] calculated with a 15 km thick ULVZ with $\Delta V_p = -10\%$, $\Delta V_s = -30\%$, and $\Delta\rho = +20\%$. The S_{ulvz} and $ScS_{ulvz}P$ amplitudes depend almost entirely on ΔV_s at the top of the ULVZ while the $S_{ulvz}P(up)$ amplitude depends on both ΔV_s and $\Delta\rho$. Note, however, that the precursors are almost not visible in the ULVZ synthetics and thus we have no sensitivity to density changes. Events 6 and 7 show some signs of a precursor but neither precursor is present in the ULVZ synthetics; these precursors would actually be better modeled by an ultra-high V_s zone (UHV_sZ). Discrepancies between the observed ScP and ULVZ synthetic ScP waveforms are most acute in the ScP codas, where the synthetics show a large arrival where none is present in the data. The amplitude of this post-cursor $ScS_{ulvz}P$ is linearly proportional to ΔV_s, such that a ULVZ with only a 10% V_s drop will be one third as large. However, none of the observed ScP waveforms appear to have this post-cursor. Instead all are more similar to the P waveforms than to the ULVZ synthetic waveforms, strongly suggesting that the CMB under the entire Gulf of Alaska is sharp and simple, confirming Vidale and Benz's (1992) localized study [8].

At layer thicknesses less than 5 km the synthetic ULVZ ScP waveforms are almost identical to the P waveforms, precluding any conclusions about thin layers based on waveform comparisons. However, regardless of thickness, a ULVZ composed of partial melt would decrease V_s and increase attenuation that would both cause smaller ScP amplitudes, in stark contrast to the large observed amplitudes.

5. Conclusion

How can we reconcile the SP_dKS and ScP observations? Possibly the simplest explanation is that no ULVZ exists under the Gulf of Alaska. As the PcP waveforms we observed are generally not visible at frequencies below 1 Hz, we did not attempt to stack them. Other PcP observations to the west of the Gulf of Alaska suggest either no ULVZ [8] or possibly an 11 km thick ULVZ just south of the Aleutian Islands [5]. No ULVZ under the Gulf of Alaska would require an ULV_pZ on the source side of the SP_dKS (Java Sea) rather than on the receiver side (Gulf of Alaska). As other SP_dKS paths within 100 km show no signs of ULVZ, this would require small-scale ULVZ structures on the order of 10–100 km. However, three-dimensional synthetics [29] show that structures with horizontal extents < 100 km produce no discernible effects on long-period waveforms such as SP_dKS.

If the SP_dKS observation is robust and a ULVZ exists below the Gulf of Alaska, one conclusion is that the ULVZ is an extremely localized 3-D structure [27] and the two data types sample different regions. However, while the long-period SP_dKS observations require a finite sized ULVZ > 100 km in horizontal extent, none of the ScP waveforms appear 'ULVZ-like' even though the ScP reflections considered here span the entire Gulf of Alaska region.

A second possibility is that the ULVZ is much thicker and has a diffuse top-boundary. However, while tomography models will overlook small-scale structures, neither V_p tomography models [14] nor P_{diff} studies [22] image anything greater than a 1–2% slow anomaly near the CMB under the Gulf of Alaska. Thus, if this is the case, we can use the resolution of the tomography models to limit the largest possible ULVZ thickness. Additionally, while the diffuse top-boundary would explain the lack of ScP waveform complications, it would create smaller ScP amplitudes, opposite of what we observe.

Possibly the SP_dKS data image only an extremely thin layer less than 5 km thick that would not be imaged by the ScP signal. The SP_dKS data do allow extremely thin layers; however, the trade-offs between thickness and density require even more drastic velocity drops [28] that would make the large ScP amplitudes even more difficult

to explain. Additionally, the Fréchet sensitivity kernels (the region to which a waveform is most sensitive) of long-period P_{diff} waves propagating over the CMB are over 100 km thick [32], suggesting that extremely thin layers will not contribute substantially to the observed long-period SP_dKS waveform.

One obvious but somewhat contradictory conclusion is that ULVZs neither have a sharp V_s change nor are partial melt but are only ultralow compressional velocity zones (ULV_pZ). If this is the case, we would need to find a chemical heterogeneity that decreases $\kappa(V_p)$ but not $\mu(V_s)$.

Acknowledgements

We appreciate conversations with K. Creager, E. Garnero, H. Paulssen, and J. VanDecar. We thank E. Garnero and A. Souriau for constructive reviews. Figures were created with GMT [33]. This research was supported by the National Science Foundation.*[AC]*

References

[1] L.G. Liu, Phase transformations and the constitution of the deep mantle, in: M. McElhinny (Ed.), The Earth: Its Origin, Structure and Evolution, Academic Press, London, 1979, pp. 177–198.
[2] E.J. Garnero, J. Revenaugh, Q. Williams, T. Lay, L.H. Kellogg, Ultralow velocity zone at the core-mantle boundary, in: The Core-Mantle Boundary Region Geodynam. Ser. vol. 28, AGU, Washington, DC, 1998, pp. 319–334.
[3] E.J. Garnero, Heterogeneity of the lowermost mantle, Annu. Rev. Earth Planet. Sci., submitted.
[4] Q. Williams, E.J. Garnero, Seismic evidence for partial melt at the base of Earth's mantle, Science 273 (1996) 1528–1530.
[5] J. Revenaugh, R. Meyer, Seismic evidence of partial melt within a possible ubiquitous low-velocity layer at the base of the mantle, Science 277 (1997) 670–673.
[6] E.J. Garnero, D.V. Helmberger, Seismic detection of a thin laterally varying boundary layer at the base of the mantle beneath the central-Pacific, Geophys. Res. Lett. 23 (1996) 977–980.
[7] E.J. Garnero, J.E. Vidale, ScP; a probe of ultralow velocity zones at the base of the mantle, Geophys. Res. Lett. 26 (1999) 377–380.
[8] J.E. Vidale, H.M. Benz, A sharp and flat section of the core-mantle boundary, Nature 359 (1992) 627–629.
[9] P.R. Cummins, R.J. Geller, N. Takeuchi, DSM complete synthetic seismograms: P-SV, spherically symmetric, case, Geophys. Res. Lett. 21 (1994) 1663–1666.
[10] B.L.N. Kennett, E.R. Engdahl, Travel times for global earthquake location and phase identification, Geophys. J. Int. 105 (1991) 429–465.
[11] A. Dziewonski, D.L. Anderson, Preliminary reference earth model, Phys. Earth Planet. Inter. 25 (1981) 297–356.
[12] S. Sipkin, Estimation of earthquake source parameters by the inversion of waveform data: Global seismicity, Bull. Seismol. Soc. Am. 76 (1986) 1515–1541.
[13] W. Kampfmann, G. Müller, PcP amplitude calculations for a core-mantle boundary with topography, Geophys. Res. Lett. 19 (1989) 653–656.
[14] H. Kárason, R.D. van der Hilst, Improving global tomography models of P-wavespeed I: Incorporation of differential times for refracted and diffracted core phases (PKP, Pdiff), J. Geophys. Res., submitted.
[15] J.C. Castle, K.C. Creager, J.P. Winchester, R.D. van der Hilst, Shear wave velocity structure at the base of the mantle, J. Geophys. Res., submitted.
[16] J.-P. Montagner, B.L.N. Kennett, How to reconcile body-wave and normal-mode reference earth models, Geophys. J. Int. 125 (1996) 229–248.
[17] Z.A. Der, High frequency P- and S-wave attenuation in the earth, Pure Appl. Geophys. 153 (1998) 273–310.
[18] B. Romanowicz, A global tomographic model of shear attenuation in the upper mantle, J. Geophys. Res. 100 (1995) 12375–12394.
[19] J. Bhattacharyya, G. Masters, P. Shearer, Global lateral variations of shear wave attenuation in the upper mantle, J. Geophys. Res. 101 (1996) 22273–22289.
[20] H.-C. Nataf, J. VanDecar, Seismological detection of a mantle plume?, Nature 364 (1993) 115–120.
[21] S.P. Grand, R.D. van der Hilst, S. Widiyantoro, Global seismic tomography: A snapshot of convection in the Earth, GSA Today 7 (1997) 1–7.
[22] M.E. Wysession, Large-scale structure at the core-mantle boundary from diffracted waves, Nature 382 (1996) 244–248.
[23] M.E. Wysession, A. Langenhorst, M.J. Fouch, K.M. Fischer, G.I. Al-Eqabi, P.J. Shore, T.J. Clarke, Lateral variations in compressional/shear velocities at the base of the mantle, Science 284 (1999) 120–125.
[24] B.L.N. Kennett, S. Widiyantoro, R.D. van der Hilst, Joint seismic tomography for bulk sound and shear wave speed in the Earth's mantle, J. Geophys. Res. 103 (1998) 12469–12493.
[25] J. Mori, D.V. Helmberger, Localized boundary layer below the mid-Pacific velocity anomaly identified from a PcP precursor, J. Geophys. Res. 100 (1995) 20359–20365.
[26] J.E. Vidale, M.A.H. Hedlin, Evidence for partial melt at the core-mantle boundary north of Tonga from the strong scattering of seismic waves, Nature 391 (1998) 682–685.
[27] L. Wen, D.V. Helmberger, Ultra-low velocity zones near

the core-mantle boundary from broadband PKP precursors, Science 279 (1998) 1701–1703.
[28] E.J. Garnero, D.V. Helmberger, Further structural constraints and uncertainties of a thin laterally varying ultra-low velocity layer at the base of the mantle, J. Geophys. Res. 103 (1998) 12495–12509.
[29] D.V. Helmberger, L. Wen, X. Ding, Seismic evidence that the source of the Iceland hotspot lies at the core-mantle boundary, Nature 396 (1998) 251–255.
[30] M. Schimmel, H. Paulssen, Noise reduction and detection of weak, coherent signals through phase-weighted stacks, Geophys. J. Int. 130 (1997) 497–505.
[31] C.H. Chapman, J. Chu, D.G. Lyness, The WKBJ seismogram algorithm, in: D.J. Doornbos (Ed.), Seismological Algorithms vol. 47, Academic Press, San Diego, CA, 1988.
[32] L. Zhao, T.H. Jordan, Three dimensional Fréchet differential kernels for seismic delay times, Geophys. J. Int., submitted.
[33] P. Wessel, W.H.F. Smith, New version of the Generic Mapping Tools released, Eos Trans. AGU 76 (1995) 329.